CFD Modelling of an Underground Water Tank Heat Storage System

M. Mahdi Salehi[1], W. Kendal Bushe[1], Paul Marmion[2] and Ray Pradinuk[2]
[1]Mechanical Engineering Department, University of British Columbia, Vancouver, BC
[2]Stantec Consulting, Vancouver, BC

Abstract

In this work, CFD is used to simulate the flow in an existing thermal labyrinth located at the basement of a hospital building. This labyrinth is an underground channel equipped with water tanks to increase the thermal mass and reduce the heating and cooling demand of the building. Thermal energy storage in the water tanks is a complex heat transfer phenomena involving turbulent forced convection, solid conduction and natural convection. The turbulent forced convection happens between the water tank outside surface and the air flow through the labyrinth. The heat is then conducted through the tank wall and induces a slow buoyant flow inside the tank. CFD techniques are used to solve these problems and the results are compared with experimental measurements. A simplified analysis is then developed to find the optimum parameters and working conditions for designing such a system in future buildings.

1 Introduction

A thermal labyrinth is a sustainable design feature that is used to increase the internal thermal mass of a building. Thermal mass helps the building store thermal energy from the diurnal variations of the outside temperature. This energy can be released with a time delay to reduce the energy consumption of the building from mechanical cooling and heating (Newell & Newell 2011). In a thermal labyrinth, outside air is drawn through the channel and the thermal energy of the flow is gained by walls, storage tanks or simple concrete blocks in the channel. The labyrinth can be located under the building to also use the earth for storage. The fluctuations of the temperature below the depth of 3 meters are significantly smaller than the surface temperature. This potential thermal energy has been used traditionally in form of a cool basement unit in buildings for warm summer conditions (Hardenberg 1982). Also, advanced earth to air heat exchangers have been used to exploit this potential energy resource for heating purposes (Ghosal, Tiwari, Das & Pandey 2005). Using a labyrinth increases the amount of energy that can be stored underground. Also, the shape of the labyrinth increases the surface area which can enhance the heat transfer rate and the performance of the system.

There is a substantially large literature on modeling the effect of thermal mass in buildings. Numerous studies, such as (Kolokotroni et al. 1998, Kalogirou et al. 2002, Braun 2003, Corgnati & Kindinis 2007, Yang & Li 2008), have focused on modeling the effect of thermal mass on reducing the cooling load of buildings in combination with Heat, Ventilation, and Air Conditioning (HVAC) systems. These works show that using thermal mass to control the cooling load of a building can result in significant savings on energy cost of the building. They have identified the effect of different parameters on the cost reduction such as climate conditions,

utility rates, occupancy schedules and control strategies. Thermal mass is also a key element in Passive houses which have been the subject of dynamic modeling works of Zhu et al. (2009) and Dodoo et al. (2012).

The above studies are focused on the external thermal mass on the building envelope such as walls and roofs. To our knowledge, the only work on simulation of the effect of an underground thermal labyrinth is that of Warwick et al. (2009). They performed a dynamic thermal modeling of a large building consisting of an art gallery and two theaters in south east England weather conditions.

All the above-mentioned studies are based on significant simplifications of the complex multi-physics phenomena in a thermal mass. The building is decomposed into a few zones for which energy balance equations are solved dynamically. This can be done by developing simple codes (Corgnati & Kindinis 2007, Yang & Li 2008) or using commercial software such as *IES - Virtural Environment* (n.d.) as used in (Kolokotroni et al. 1998, Warwick et al. 2009) and TRNSYS (*Transient System Simulation Tool* n.d.) as used in (Kalogirou et al. 2002). The accuracy of this type of simulation is dependent on the heat transfer coefficients of the walls in each zone. These values are usually determined by simple empirical relations. An alternative is using detailed Computational Fluid Dynamics (CFD) tools to increase the accuracy of the predictions.

Detailed fluid flow and heat transfer mechanisms in a thermal labyrinth can be better modeled using CFD tools. CFD is an alternative to the existing correlations for calculation of the convective heat transfer coefficient of buildings (Defraeye et al. 2011). Turbulent flow structures in building-related applications such as flow around building envelopes and inside a labyrinth channel involve large scale turbulent coherent structures introducing unsteady flow effects and complicated vortical structures (Yakhot et al. 2006). The convective heat transfer rate is affected by these scales. Reynolds-Averaged Navier Stokes (RANS) and Large-Eddy Simulation (LES) turbulence models can be used to model the effect of these scales. Laboratory scale experimental data are available to test the performance of these turbulence models in building related applications such as the experiments of Meinders et al. (1999). This work has been the subject of CFD simulations using RANS (Defraeye et al. 2010) and LES turbulence models (Tyacke & Tucker 2012). An important factor in these simulations is the resolution of the thermal and viscous boundary layers on the walls. If the computational grid resolution is not fine enough, turbulent wall functions need to be used (Allegrini et al. 2012). Hybrid RANS and LES turbulence models can be used to reduce the computational cost of CFD simulations while having reasonable accuracy (Spalart 2000).

In this work, the dynamic thermal performance of a water tank heat storage system in an underground labyrinth is analyzed. The labyrinth is first briefly explained in section 2. The CFD simulation is then presented in section 3. In section 4, the experimental analysis and results are explained. Finally, a simplified analytical methodology is used in section 5 to identify the most critical parameters for future design of such a system.

2 NRH Labyrinth

The Nanaimo Regional Hospital thermal labyrinth is an underground channel with concrete walls. The schematic of the labyrinth is shown in Figure 1. It is located under the building in the basement. From one end, the labyrinth is connected to the outside air and from another end, it is connected to the air-handling units' intake ducts. This labyrinth is used for pre-heating and pre-cooling of the outside air. The channel is equipped with slim water tanks to further increase the thermal mass of the labyrinth. Figures 1 and 2 show the location of water tanks in

the channel. The water tanks are made of polyethylene plastic material. Each tank is filled with 1022 litres of tap water.

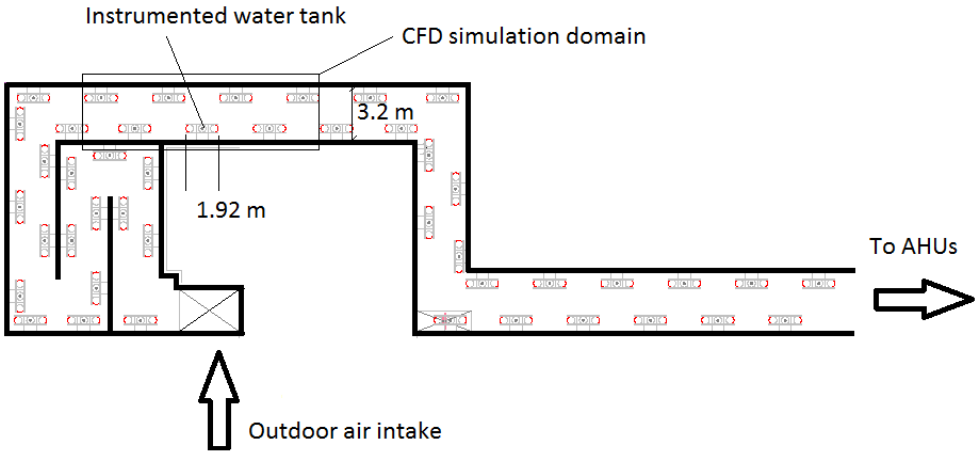

Figure 1: Schematic of the Nanaimo Regional Hospital thermal labyrinth designed by Stantec Consulting.

Figure 2: Water tanks in underground thermal labyrinth at Nanaimo Regional Hospital

This labyrinth is now in operation. A measurement and verification study is currently being done to evaluate the energy savings of this heat storage system. The objective of this study is to develop predictive modeling approaches for future design of such a system for different building types in various climate conditions. The critical element of this labyrinth is the water tank heat storage system. The main focus of this paper is on using CFD techniques to predict the dynamic behavior of water tanks. A simplified analytical approach is then developed for future design of such systems.

3 Modeling

The dynamic thermal characteristics of the water tanks can be represented in gross terms by the following equation:

$$\dot{Q} = -C\frac{dT_w}{dt} = \frac{1}{R_{eff}}(T_w - T_a) \tag{1}$$

where, $\dot{Q}$ is the heat flux from the water tank to the air flow, C is the heat capacity of the tank, T_w is the average water temperature inside the tank and T_a is the air reference temperature. The

effective R-value of the tank, R_{eff}, depends on three different physical phenomena: turbulent forced convection heat transfer between the tank surface and the air stream, solid conduction heat transfer in the polyethylene tank wall and natural convection of the water flow inside the tank. CFD can be used to calculate both forced and natural convection heat transfer phenomena. These two phenomena are effectively decoupled due to having substantially different time scales. Thus, the air flow simulations are first performed to calculate the air film R-value. Then, this R-value is used to calculate the natural convection heat transfer inside the water tank with an approximation for conduction heat transfer through the polyethylene walls. The OpenFOAM (2013) software package is used for these CFD modelings. OpenFOAM is an open-source tool for solving partial differential equations with many different physical sub-models.

Air Flow Modeling

The *rhoSimpleFoam* solver of OpenFOAM is used for simulation of turbulent convection heat transfer. This is a compressible solver that solves continuity, Navier-Stokes and conservation of energy equations. The standard k-ε turbulence model is used (Launder & Spalding 1974). The `kqRWallFunction` turbulence wall function available in OpenFOAM is used for k, `epsilonWallFunction` is used for ε and `mutkWallFunction` is used for turbulent viscosity. This combination of wall functions result in imposing the zero gradient condition for turbulent kinetic energy on the wall and setting the ε and turbulent viscosity based on the logarithmic law of the wall. Also, the production term for turbulent kinetic energy transport equation is modified near the wall (Versteeg & Malalasekera 2007). The problem is solved with a steady-state assumption and the SIMPLE algorithm for pressure corrections (Patankar & Spalding 1972). The total mass flow rate is set at the inlet boundary condition.

Validation Case

In order to validate the turbulent heat transfer modeling approach, a turbulent air boundary layer over a heated flat plate is simulated. Seban & Doughty (1956) proposed the following correlation for the non-dimensional heat transfer coefficient (Nusselt number):

$$Nu_x = \frac{h_x x}{k_a} = 0.0236\, {Re_x}^{4/5} \tag{2}$$

where h_x is the local convection heat transfer coefficient $h_x = \dot{Q}/A(T_w(x) - T_a)$, x is the spatial dimension starting from the flat plate leading edge, k_a is the air conduction heat transfer coefficient and $Re_x = \rho u x/\mu$ is the local Reynolds number. The CFD code described above is used to calculate the local heat flux. The simulation results are shown in Figure 3. According to this figure, the CFD approach slightly under-predicts the heat transfer rate. The local heat flux is integrated over x to obtain the overall heat transfer rate over the flat plate. There is 15% discrepancy between the experimental and the CFD results in overall heat transfer rate in this validation case.

Labyrinth Section Case

Only a section of the labyrinth is simulate to calculate the tank air film R-value. This section is shown in Figure 1. The tanks have a 1.92 m length and 1.92 m height. The geometry of this section of the labyrinth is modeled in NX Unigraphics. This geometry is then exported to be used by the *SnappyHexMesh* grid generation utility of OpenFOAM. This utility generates an unstructured mesh (hexahedra, prisms, wedges, pyramids, tetrahedra and polyhedra) from an

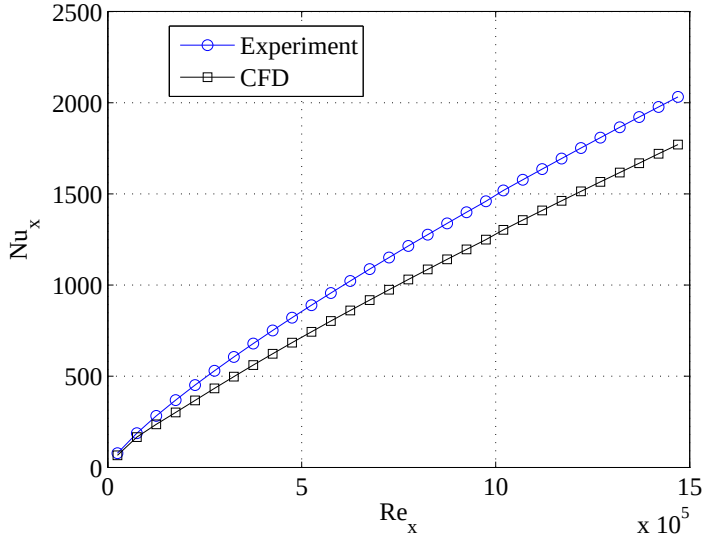

Figure 3: Heat transfer coefficient as a function Reynolds number for turbulent convection heat transfer over a heated flat plat.

arbitrary three-dimensional CAD surface. Figure 4 shows the details of the surface mesh in a section of the labyrinth.

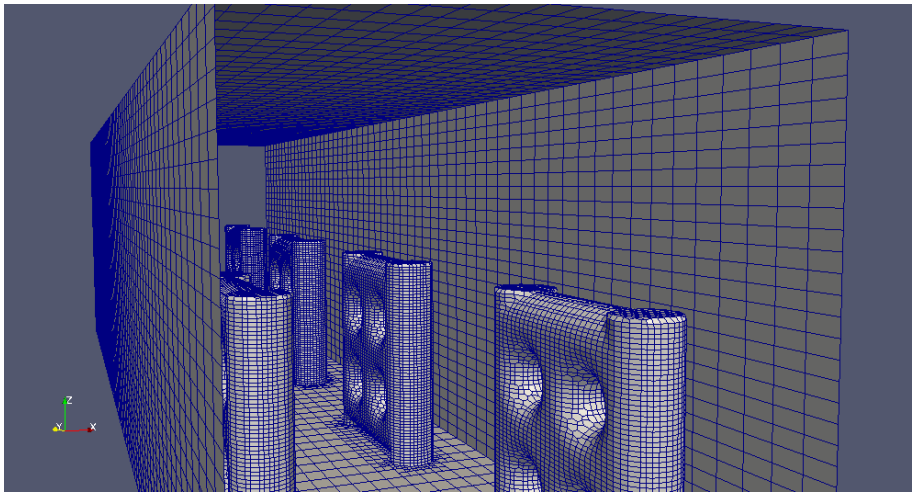

Figure 4: Mesh details of the tank and channel wall surfaces.

The flow rate of each AHU is measured and logged in the building monitoring system. Simulations are performed with two flow rates: 10,000 CFM and 20,000 CFM. A constant velocity inlet boundary condition is used to impose these flow rates.

In order to calculate the air film R-value, the temperature of one of the tanks (the control tank) is changed relative to the air flow temperature from $0^{\circ}C$ to $20^{\circ}C$. The heat transfer between the tank and the concrete slab is ignored. It is assumed that the concrete slab has the same surface temperature as the surrounding air temperature. The simulations are performed with different grids to ensure that the results are independent of the grid. The results of the finest grid are shown here.

Figure 5 shows the contour plot of the heat flux on the control tank. According to this figure, the heat flux is higher on the leading face of the tank where the flow is impinging on the surface. The total heat flux is plotted vs. the temperature gradient in Figure 6. The inverse of

the slope is the air film R-value: $R_{air\ film} = \Delta T / \dot{Q}$.

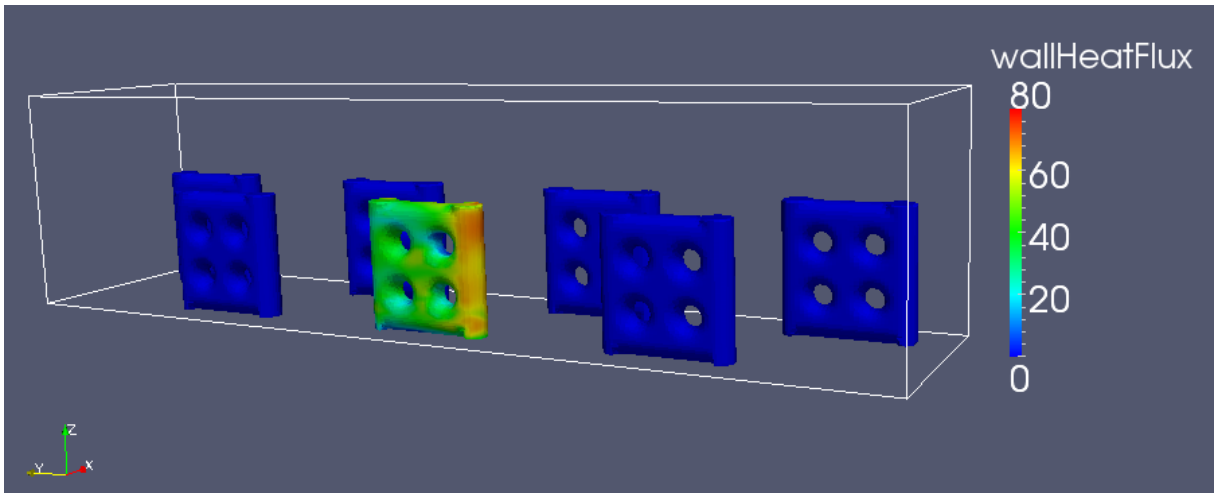

Figure 5: The heat flux on the tank with different surface temperature.

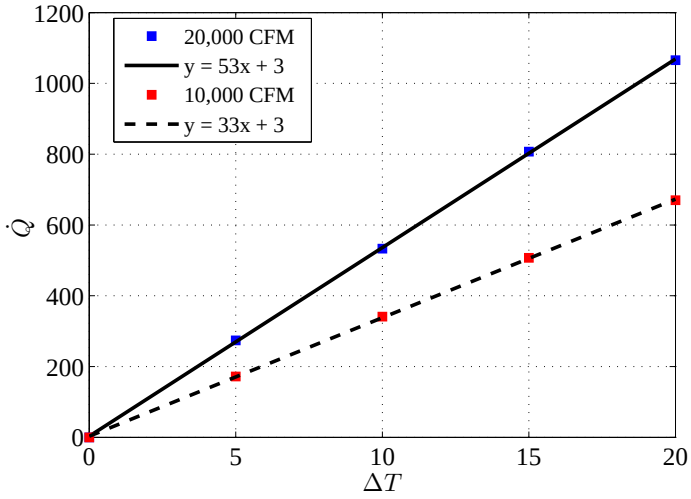

Figure 6: The total wall heat flux vs. temperature difference between the tank surface temperature and the air temperature.

Water Flow Modeling

In order to simulate the buoyant flow in the tank, the inside volume of the tank is meshed. The *buoyantBoussinesqPimpleFoam* solver of OpenFOAM is used for this simulation. This is an unsteady solver with a Boussinesq approximation for modeling the buoyancy effect. This approximation is valid for low Mach number flows. This is a pressure-based solver that uses PIMPLE algorithm for pressure corrections(OpenFOAM 2013). PIMPLE algorithm is a combination of SIMPLE and PISO (Ferziger & Peri 2002) algorithm for unsteady flows. Since the temperature gradients are not high enough, the flow velocity scale due to the buoyancy effect is low. Therefore, the flow field is laminar. This simulation only has no-slip wall boundary type. In order to model the convection and conduction heat transfer into the tanks, a Robin-type boundary condition is imposed on the walls for temperature:

$$k\frac{\partial T}{\partial n} = h(T - T_a) \tag{3}$$

where T is wall temperature, $\frac{\partial T}{\partial n}$ is the temperature gradient normal to the wall, k is the conduction heat transfer coefficient of the polyethylene, h is the convection heat transfer coefficient of the air film ($1/R_{air\ film}$) and T_a is the air temperature. Using this boundary condition, the temperature distribution inside the tank can be simulated by changing the surrounding air temperature.

The water flow field is initialized with $T = 300\ K$. The air temperature is set to $T_a = 310\ K$ at $t = 0$. The unsteady motion of the water flow inside the tank is simulated for 24 hours. Figure 7 shows the contour plot of the surface temperature after 5 hours. This figure shows the temperature stratification throughout the tank due to the non-linear hydrodynamic buoyant flow. Using the above initial and boundary conditions, the simplified model of equation 1 has

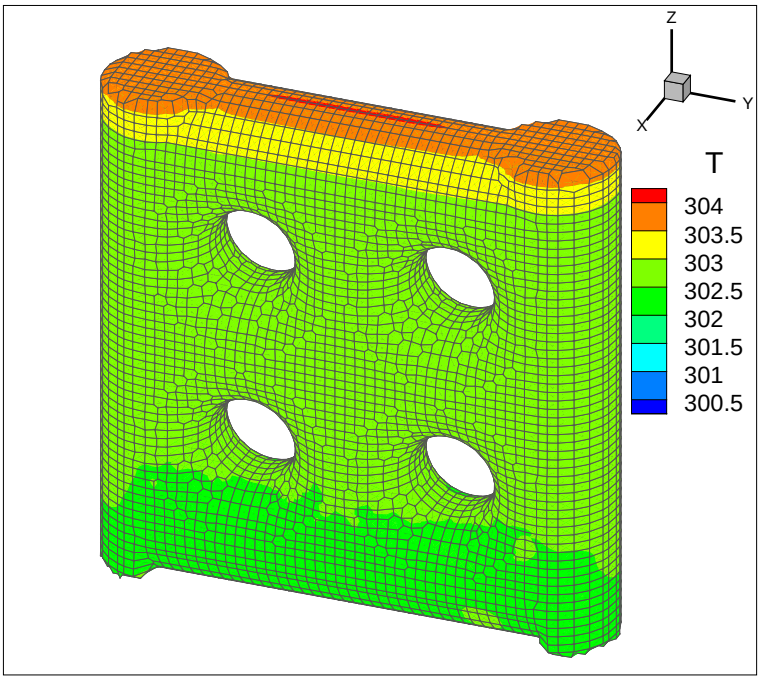

Figure 7: Surface mesh and temperature contour plot of water at t=5h

the following analytical solution:

$$\frac{T_a - T_w(t)}{T_a - T_w(0)} = e^{-t/\tau} \tag{4}$$

where $\tau = R_{eff}C$ is the characteristic time constant. The averaged water temperature of the CFD calculations can be used in the above equation to calculate the overall time constant for thermal charging and discharging of the tanks. Figure 8 shows the temporal variation of the average water tank temperature. Error bars represent twice the volume-averaged variance of the temperature: $\overline{T''^2} = \int (\overline{T}_w^2 - \overline{T}_w^2) dV / \int dV$. An exponential curve of the form of equation 4 is fitted to the average temperature results as shown in Figure 8. This curve fit gives a value of $\tau = 22.7\ h$ for the time constant.

4 Experimental Results

This labyrinth is instrumented for dynamic control and long-term performance assessment. There are two temperature sensors inside the labyrinth for air temperature measurement and one temperature sensor inside one of the tanks. The location of the temperature sensors are shown in Figure 9. One of the air temperature sensors is upstream of the instrumented tank.

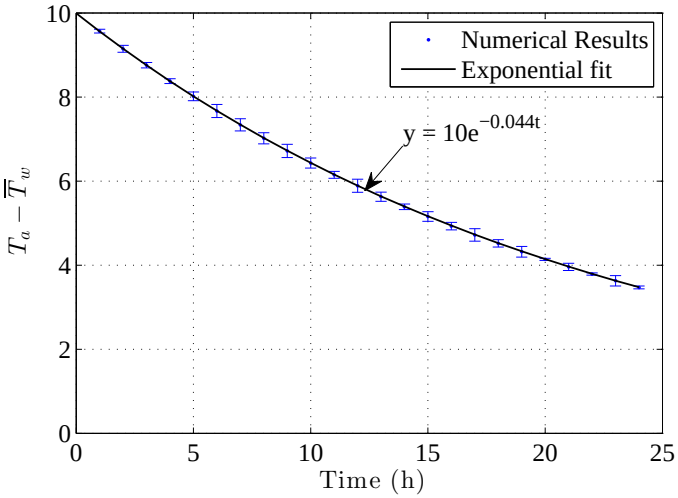

Figure 8: Temporal response of the average water tank temperature to the step change of the surrounding air temperature. Error bars represent twice of the temperature variance.

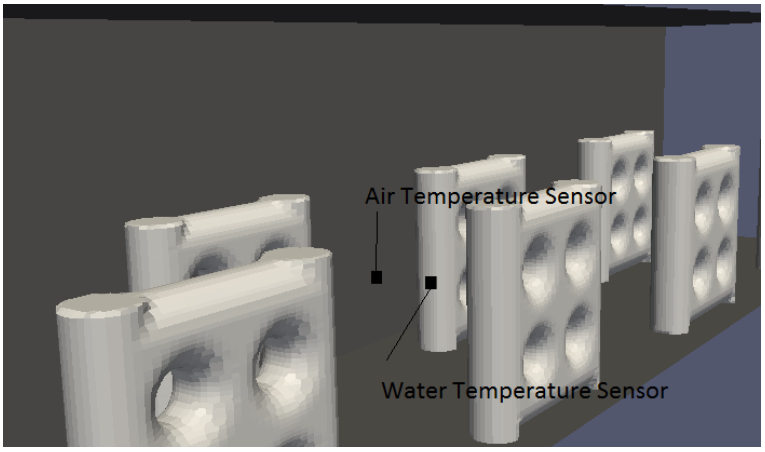

Figure 9: Locations of the temperature sensors.

This air temperature sensor is attached to the wall and does not provide the average air temperature upstream of the tank. Nevertheless, the output of this sensor and the water temperature sensor are used to approximate the time constant of the water tanks. Figure 10 shows the diurnal variation of the air and water temperature sensors for the date of 29/10/2013 – selected due to the relatively high diurnal temperature variation that day. The instrumented water tank is located far downstream of the labyrinth outdoor air intake. Temperature variation in the labyrinth decreases as the distance from the intake increase due to the thermal mass buffering effect.

The temperature data are used in equation 1 to find the time constant. The water temperature temporal derivative can be calculated numerically using a simple 2^{nd}-order central scheme. However, such a numerical integration can amplify the measurement error. In order to alleviate this, a 6^{th}-order polynomial is fitted to the water temperature data as shown in Figure 10. The goodness of fit is $R^2 = 0.99$. This polynomial is used to analytically calculate the derivative. The difference between the water temperature and the air temperature is plotted against this derivative in Figure 11. These two parameters are linearly correlated; the slope of the fitted line is the time constant: $\tau \approx 11.2\ h$.

The experimental result for the time constant is significantly different from the model

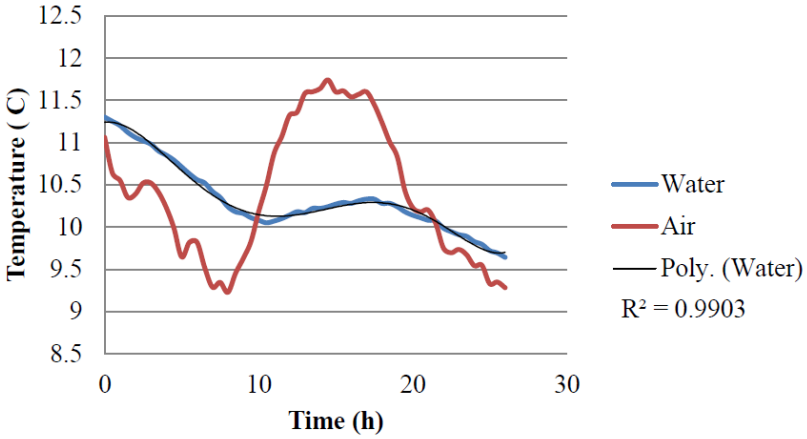

Figure 10: Storage tank water temperature and air flow temperature.

prediction in the previous section. This is likely in part due to the inconsistencies in the reference air temperature between the two calculations. As mentioned above, the air temperature is only measured at one point close to the labyrinth concrete wall. Ideally, the average air temperature needs to be measured as well. Also, the flow rate sensors are based on the pressure difference across the AHU supply fans. Further measurement is required to ensure the accuracy of these sensors.

At the same time, there are some important simplifications in the simulations. The heat transfer between the concrete wall and the water tank is ignored. As shown in Figure 2, the tanks are located on the concrete slabs without any insulation. Therefore, there exists a conduction heat transfer that depends on the contact resistance and the slab temperature. This information is not currently available and will be addressed in future work. Another source of modeling error is the underlying turbulence model in the air flow simulation. The tanks are inducing large scale turbulent structures in the flow field; Large-Eddy Simulation (LES) of the air flow is likely to improve the results.

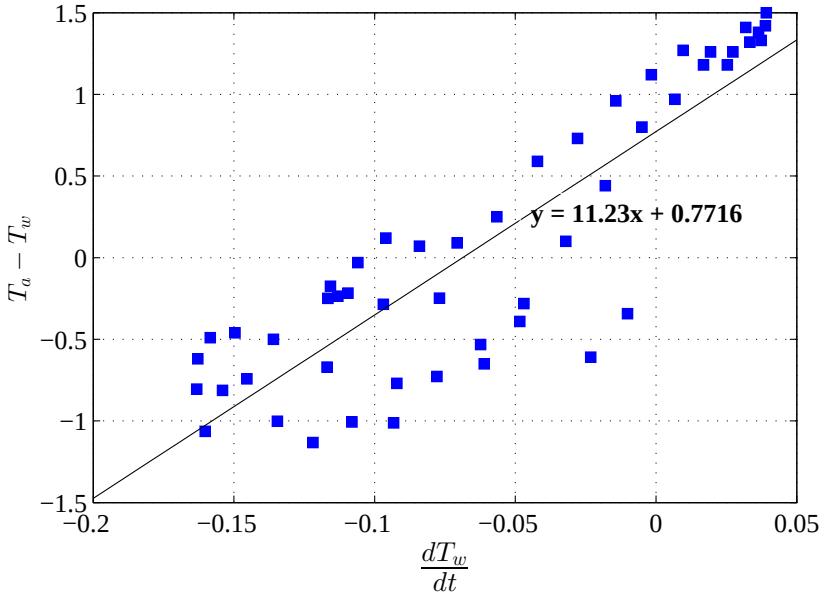

Figure 11: The correlation between the air-water temperature difference and the rate of water temperature change

5 Future Designs

In this section a simplified mathematical approach is used to find the optimum time constant and operating condition for future design of a thermal labyrinth. Equation 1 has an analytical closed form solution for average water temperature as a function of the air temperature:

$$T_w(t) = \frac{1}{\tau} e^{-t/\tau} \int e^{t/\tau} T_a(t) dt \tag{5}$$

where $\tau = R_{eff}C$. For simplicity, a cosine harmonic functional form is assumed for the air temperature diurnal variation:

$$T_a = T_0 - \delta \cos(\omega t) \tag{6}$$

where T_0 is the average daily temperature, $\omega = \pi/12$ and t is the time in hours; δ is the fluctuation amplitude which is half of the difference between the maximum and minimum daily temperature. Substituting equation 6 into equation 5, after integration and some simplifications, the following equation is obtained for the water tank temperature:

$$T_w = T_0 - \delta^* \cos(\omega t - \theta) - \frac{\delta \tau^2 \omega^2}{1 + \tau^2 \omega^2} e^{-t/\tau} \tag{7}$$

The last term is the result of initial conditions and damps out quickly. The water temperature fluctuation amplitude δ^* and the phase delay θ are as follows:

$$\begin{aligned} \delta^* &= \frac{\delta}{\sqrt{1 + \tau^2 \omega^2}} \\ \theta &= \sin^{-1}\left(\frac{\tau \omega}{\sqrt{1 + \tau^2 \omega^2}}\right) \end{aligned} \tag{8}$$

These equations show that increasing τ results in decreasing the water tank temperature fluctuation amplitude. This is the case when either the capacity or R-value is large. The phase delay represents the buffering effect of the thermal mass. This number starts from $\theta = 0$ for $\tau = 0$ and increases with increasing τ. It asymptotically approaches $\theta = \pi/2$ as $\tau \to \infty$.

Substituting equation 7 into 1, the heat transfer rate from the water tank to labyrinth air flow can be calculated:

$$\dot{Q} = \frac{1}{R_{eff}} \left[\delta^* \cos(\omega t - \theta) - \delta \cos(\omega t)\right]. \tag{9}$$

According to this equation the heat transfer rate is inversely proportional to R_{eff}. However, for a constant capacity, increasing R_{eff} results in increasing τ which enhances the buffering effect of the thermal mass. In other words, the heat release happens when the air temperature is decreasing and the thermal mass absorbs air flow heat when the temperature is increasing. This effect is shown in Figure 12 for a daily averaged air temperature of $T_0 = 10^\circ C$ and fluctuation amplitude of $\delta = 5^\circ C$. This figure suggests that there is an optimum value for the time constant τ that gives the best performance for the water tanks in the labyrinth.

The optimum performance of the water tanks also depends on the AHU set point temperature – relative to the mean outside air temperature – and the additional fan power due to the presence of the tanks inside the channel. This extra fan power is related to the aerodynamic drag force of the tank:

$$P = \eta \dot{V} \frac{F_D}{A} \tag{10}$$

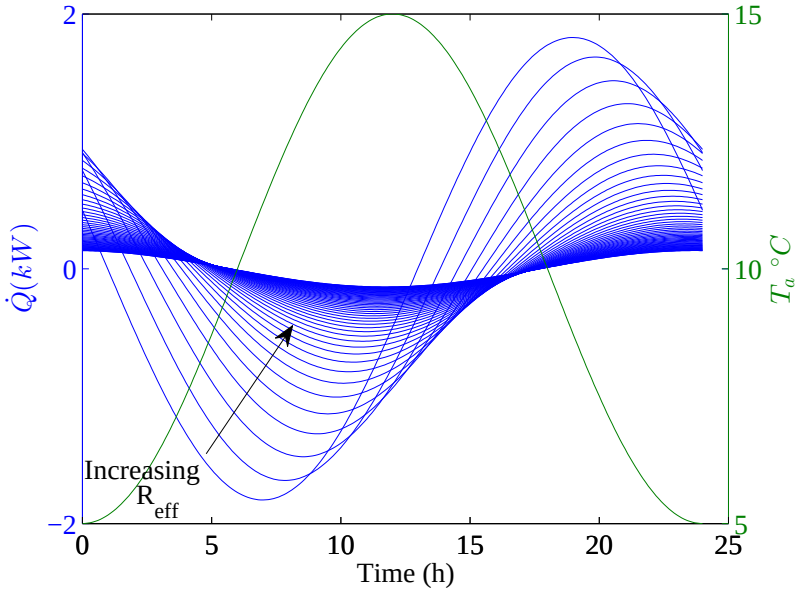

Figure 12: Effect of changing the tank R-value on the diurnal heat flux from the tank.

where η is the fan efficiency, $\dot{V}$ is the volumetric flow rate through the labyrinth, A is the cross section area of the labyrinth and F_D is the drag force. This force can be easily obtained using the CFD model described in section 3. Knowing this parameter and the heat transfer rate, one can define a daily cooling and heating performance factor for the water tanks in the labyrinth:

$$PF = \int_{t_1}^{t_2} \dot{Q}dt \Big/ \int_{0}^{24} Pdt \tag{11}$$

where $[t_1, t_2]$ is the time frame when the air temperature is higher than the set-point temperature ($T_a > T_{set}$) for cooling performance factor. For the water tanks simulated in section 3, the drag force is $F_D = 0.8\,N$. Assuming a fan efficiency of $\eta = 0.7$, the daily cooling performance factor is calculated. Figure 13 shows the contour plot of this parameter for $\delta = 5^\circ C$ as a function of the time constant and the AHU set-point temperature.

Figure 13 shows that the optimum value for the time constant is around 4 hours independent of the operating conditions. Also, this figure shows that the optimum performance happens when the average daily temperature is equal to the set-point temperature ($T_0 = T_{set}$); in such a case, there is a balance between cooling and heating capacity that can be buffered by the thermal mass effect of the labyrinth. On the other hand, as the difference between the mean daily temperature and the AHU set-point temperature increases, the performance of the labyrinth decreases. The above figure is for high outside air temperature fluctuations ($\delta = 5^\circ C$) which is not always the case. Also as mentioned above, the water tanks that are further downstream in the labyrinth are experiencing much smaller air temperature fluctuations. Therefore, under certain operating conditions the additional fan electricity consumption is higher than the thermal energy savings.

6 Conclusion and Future Work

In this work, the dynamic performance of a water tank heat storage system in a building thermal labyrinth was investigated. The critical parameter in the dynamic behavior of a thermal labyrinth is the time constant which is a characteristic time scale for the charging and discharging of thermal energy. This parameter was numerically and experimentally investigated. The

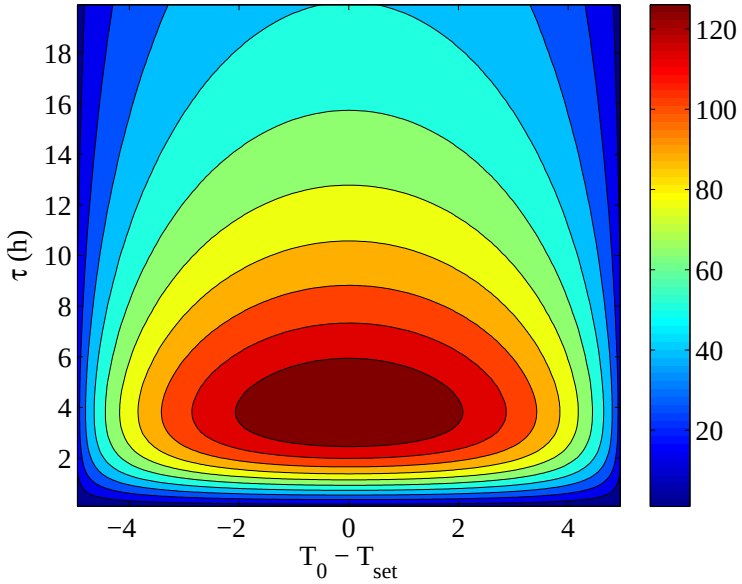

Figure 13: The daily cooling performance factor of the water tank for $\delta = 5°C$

numerical approach comprises of two different CFD models: for the air flow and the buoyant water flow. In the experimental approach, the water and air temperature are measured for a period of one day and used to approximate the time constant. There is a significant difference between the results of these two approaches and, in future work, we hope to address this discrepancy. More instrumentation such as averaging sensors for the air temperature and more accurate flow rate sensors will be installed in the labyrinth. Also, another water tank closer to the labyrinth intake will be equipped with temperature sensors to enhance the temperature variation resolution. The simulations will also be further developed with a better turbulence model and considering the conduction heat transfer between the tanks and the concrete slabs.

7 Acknowledgment

The financial support of NSERC and Sustainable Building Science Program is greatly appreciated. Also, the authors wish to thank Stantec Consulting and the Vancouver Island Health Authority for making design and operational data available.

8 References

Allegrini, J., Dorer, V., Defraeye, T. & Carmeliet, J. (2012), 'An adaptive temperature wall function for mixed convective flows at exterior surfaces of buildings in street canyons', *Building and Environment* **49**(0), 55 – 66.

Braun, J. E. (2003), 'Load control using building thermal mass', *Journal of Solar Energy Engineering* **125**(3), 292–301.

Corgnati, S. P. & Kindinis, A. (2007), 'Thermal mass activation by hollow core slab coupled with night ventilation to reduce summer cooling loads', *Building and Environment* **42**(9), 3285 – 3297.

Defraeye, T., Blocken, B. & Carmeliet, J. (2010), 'CFD analysis of convective heat transfer at the surfaces of a cube immersed in a turbulent boundary layer', *International Journal of Heat and Mass Transfer* **53**(1-3), 297–308.

Defraeye, T., Blocken, B. & Carmeliet, J. (2011), 'Convective heat transfer coefficients for exterior building surfaces: Existing correlations and CFD modelling', *Energy Conversion and Management* **52**(1), 512–522.

Dodoo, A., Gustavsson, L. & Sathre, R. (2012), 'Effect of thermal mass on life cycle primary energy balances of a concrete- and a wood-frame building', *Applied Energy* **92**(0), 462 – 472.

Ferziger, J. H. & Peri, M. (2002), *Computational Methods for Fluid Dynamics*, Springer London, Limited.

Ghosal, M., Tiwari, G., Das, D. & Pandey, K. (2005), 'Modeling and comparative thermal performance of ground air collector and earth air heat exchanger for heating of greenhouse', *Energy and Buildings* **37**(6), 613 – 621.

Hardenberg, J. G. V. (1982), 'Considerations of houses adapted to local climate a case study of iranian houses in yazd and esfahan', *Energy and Buildings* **4**(2), 155 – 160.

IES - Virtural Environment (n.d.), `http://www.iesve.com`.

Kalogirou, S. A., Florides, G. & Tassou, S. (2002), 'Energy analysis of buildings employing thermal mass in cyprus', *Renewable Energy* **27**(3), 353 – 368.

Kolokotroni, M., Webb, B. & Hayes, S. (1998), 'Summer cooling with night ventilation for office buildings in moderate climates', *Energy and Buildings* **27**(3), 231 – 237.

Launder, B. E. & Spalding, D. B. (1974), 'The numerical computation of turbulent flows', *Computer Methods for Applied Mechanics and Engineering* **3**(2), 268 – 289.

Meinders, E., Hanjalic, K. & Martinuzzi, R. (1999), 'Experimental study of the local convection heat transfer from a wall-mounted cube in turbulent channel flow', *Journal of Heat Transfer-Transactions of the ASME* **121**(3), 564–573.

Newell, T. & Newell, B. (2011), 'Thermal Mass Design', *ASHRAE Journal* **53**(3), 70+.

OpenFOAM (2013), *The open source CFD Toolbox*, OpenFOAM Foundations, http://www.openfoam.org/.

Patankar, S. V. & Spalding, D. B. (1972), 'A calculation procedure for heat, mass and momentum transfer in three-dimensional parabolic flows', *International Journal of Heat and Mass Transfer* **15**(10), 1787–1806.

Seban, R. A. & Doughty, D. L. (1956), 'Heat transfer to turbulent boundary layers with variable free-stream velocity', *Journal of Heat Transfer* **78**, 217223.

Spalart, P. (2000), 'Strategies for turbulence modelling and simulations', *International Journal of Heat and Fluid Flow* **21**(3), 252 – 263.

Transient System Simulation Tool (n.d.), `http://www.trnsys.com`.

Tyacke, J. & Tucker, P. (2012), 'LES of heat transfer in electronics', *Applied Mathematical Modelling* **36**(7), 3112 – 3133.

Versteeg, H. K. & Malalasekera, W. (2007), *An introduction to computational fluid dynamics: the finite volume method*, Pearson Education Ltd., Harlow, England; New York.

Warwick, D. J., Cripps, A. J. & Kolokotroni, M. (2009), 'Integrating active thermal mass strategies with HVAC systems: Dynamic thermal modelling', *International Journal of Ventilation* **7**(4), 345–367.

Yakhot, A., Anor, T., Liu, H. & Nikitin, N. (2006), 'Direct numerical simulation of turbulent flow around a wall-mounted cube: spatio-temporal evolution of large-scale vortices', *Journal of Fluid Mechanics* **566**, 1–9.

Yang, L. & Li, Y. (2008), 'Cooling load reduction by using thermal mass and night ventilation', *Energy and Buildings* **40**(11), 2052 – 2058.

Zhu, L., Hurt, R., Correia, D. & Boehm, R. (2009), 'Detailed energy saving performance analyses on thermal mass walls demonstrated in a zero energy house', *Energy and Buildings* **41**(3), 303 – 310.